Published in final edited form as:

Cancer Res. 2020 June 15; 80(12): 2550–2563. doi:10.1158/0008-5472.CAN-19-3718.

EIF3H orchestrates Hippo pathway-mediated oncogenesis via catalytic control of YAP stability

Zhuan Zhou[1,*], **Honghong Zhou**[2,*], **Luca Ponzoni**[3,*], **Aiping Luo**[2], **Rui Zhu**[2], **Mingjing He**[4], **Yi Huang**[4], **Kun-Liang Guan**[5], **Ivet Bahar**[3], **Zhihua Liu**[2,§], **Yong Wan**[1,§]

[1]Department of Obstetrics and Gynecology, Department of Pharmacology, The Robert H. Lurie Comprehensive Cancer Center, Northwestern University Feinberg School of Medicine, Chicago, IL 60611

[2]State Key Laboratory of Molecular Oncology, National Cancer Center/Cancer Hospital, Chinese Academy of Medical Sciences and Peking Union Medical College, Beijing 100021, China

[3]Department of Computational and Systems Biology, University of Pittsburgh School of Medicine, PA 15213

[4]UPMC Hillman Cancer Center, University of Pittsburgh School of Medicine, Pittsburgh, PA 15213

[5]Department of Pharmacology, Moores Cancer Center, University of California at San Diego, La Jolla, CA 92093

Abstract

EIF3H is presumed to be a critical translational initiation factor. Here our unbiased screening for tumor invasion factors has identified an unexpected role for EIF3H as a deubiquitylating enzyme that dictates breast tumor invasion and metastasis by modulating the Hippo-YAP pathway. EIF3H catalyzed YAP for deubiquitylation, resulting in its stabilization. Structure-based molecular modelling and simulations coupled with biochemical characterization unveiled a unique catalytic mechanism for EIF3H in dissociating polyubiquitin chains from YAP through a catalytic triad consisting of Asp90, Asp91, and Gln121. Trp119 and Tyr 140 on EIF3H directly interacted with the N-terminal region of YAP1, facilitating complex formation of EIF3H and YAP1 for YAP1 deubiquitylation. Stabilization of YAP via elevated EIF3H promoted tumor invasion and metastasis. Interference of EIF3H-mediated YAP deubiquitylation blocked YAP-induced tumor progression and metastasis in breast cancer models. These findings point to a critical role for YAP regulation by EIF3H in tumor invasion and metastasis.

Keywords

EIF3H; YAP; ubiquitylation; Hippo pathway and tumor metastasis

[§]**Corresponding authors:** Yong Wan, Tel.: 312-503-2769; Fax: 312-503-0095; yong.wan@northwestern.edu; Zhihua Liu, Tel: 86-10-67723789; Fax: 86-10-67723789; liuzh@cicams.ac.cn.

[*]These authors contributed equally to this manuscript

Conflict of interest: The authors declare no potential conflicts of interest.

INTRODUCTION

Malignant tumor invasion spreads tumor cells to distal vital organs and is a pivotal step leading to cancer death. YAP-mediated Hippo cascade is thought to be a critical signaling pathway in regulating cellular events during tumor invasion and metastasis, including epithelial-mesenchymal transition (EMT), cell migration, anoikis and cancer stem cell expansion (1–3). It has been previously demonstrated that the Hippo pathway is tightly modulated by the ubiquitin-proteasome system (UPS) (4–6). The signaling-induced modulation for several Hippo pathway components, such as LATS, YAP/TAZ, AMOT, MOB1 and SAV1, has been linked to ubiquitin-protein ligases, including β-TRCP/SCF, ITCH, WWP1, PRAJA, SIAH2, $CRL4^{CDAF1}$and FBW7 (6–9). Malfunction in the proteolytic regulation of Hippo signaling leads to a variety of human diseases including cancer (10,11). Thus far, great efforts have been made to investigate how Hippo signaling modules are regulated by E3 ligase for ubiquitylation followed by degradation (6). However, how the family of deubiquitinating enzymes (DUBs) impacts the Hippo signaling and how their deregulation contributes to oncogenesis remain less well understood until recently (5,12).

Targeting UPS is appreciated as a new therapeutic strategy in treating diseases (13). Many vital small molecule inhibitors that block various E3 ligases and proteasome have been recently applied to anti-cancer therapy (13), while the potential for deubiquitinases as ideal therapeutic targets is just beginning to attract attention in the field. Principally, the 100 DUBs in the human genome can be divided into six families, including ubiquitin-specific proteases (USPs), ubiquitin COOH-terminal hydrolases (UCHs), ovarian tumor proteases (OTUs), Josephins, the JAB1/MPN/MOV34 family (JAMMs) and motif interacting with ubiquitin-containing novel DUB family (MINDYs) (14). Biochemical characterization has unveiled that the catalytic effect of most DUBs is mediated by their cysteine isopeptidase function. One general exception is the JAMMs family whose catalytic function is exclusively facilitated by histidine coordinated zinc metalloproteases (15). Results from mouse genetics and biochemical studies have revealed the importance of DUBs, such as ODUT7B, USP7 and USP10, in regulating oncogenesis (16,17).

To systematically evaluate the impact of the individual members of the DUB family in triggering tumor initiation and promoting tumor invasion, we have screened 100 DUBs by utilizing both tumor malignant transformation and tumor invasion assays and identified several candidate DUBs (18). Among these, EIF3H was observed to be the most potent in promoting tumor invasion. Previous works have extensively described the impact of EIF3H in regulating protein translation, where EIF3H is one of the subunits of eukaryotic translation initiation factor 3 (eIF-3) complex that comprises 13 non-identical protein subunits and functions at several steps in the initiation of protein synthesis (19). EIF3H and EIF3F, another subunit of the eIF-3 complex, are also classified to the JAMM family of deubiquitinases for their common feature of non-conserved MPN domains. Amplification and overexpression of EIF3H have been confirmed in multiple cancers, including breast cancer (20–23). Elevated EIF3H has been reported to associate with tumorigenesis and drug sensitivity (21,24,25). However, whether EIF3H acts as a deubiquitinase and if its putative MPN domain is active that regulates carcinogenesis remain unknown.

In this study, we report that EIF3H is a potent tumor invasion and metastasis promoting factor through an unbiased screening. Under oncogenic circumstances, EIF3H directly interacts with YAP and catalyzes the removal of poly-ubiquitin chain on YAP, resulting in YAP stabilization and its transactivation (4). Our findings establish a previously undocumented catalytic role for EIF3H as a deubiquitinase that stabilizes YAP and promotes tumor invasion and metastasis.

MATERIALS AND METHODS

Cell lines and cell culture

HEK293T, 184-B5, MCF10A, MCF10F, MDA-MB-231, MDA-MB-468, HCC1937, HCC38, MCF-7, T47D, SKBR3 and BT474 cells were obtained from the American Type Culture Collection (Manassas, VA). All cell lines were Mycoplasma tested every 3 months using MycoProbe Mycoplasma Detection Kit (R&D Systems). The length of time between cell line thawing and use in experiment did not exceed 1 month (two or more passages). The retroviral packaging line Phoenix-A cells were the gift from Edward V. Prochownik. The tamoxifen resistance cell line HTR was from Dr. David R Gius. The metastatic cell lines including bone metastasis 231-BoM-1833 (BoM-1833), brain metastasis 231-BrM2-831 (BrM2-831) and lung metastasis 231-LM2-4175 (LM2-4175) were obtained from Dr. Joan Massage.

Tissue specimens

268 breast invasive ductal carcinoma and 22 pairs of primary cancer and adjacent normal tissue specimens were analyzed. The 22 pairs of tissue were obtained from patients who were treated with surgical resection alone in 2014 at the Cancer Hospital Chinese Academy of Medical Science. None of the patients had received radiotherapy or chemotherapy before surgery. The specimens were immediately fixed in 4% polyformaldehyde and completely embedded in paraffin (18,26). Clinical characteristics of the patients are summarized in Table S2.

Mice experiment

For 4T1 spontaneous metastasis mice model, $5x10^5$ cells 4T1 cells in PBS were injected into the Balb/C mice mammary fat pad. When tumors are palpable, tumor growth was measured for 3 weeks and calculated as 0.52 x L x W x W. 4 weeks after tumor injection, the xenograft tumor and mice lung were collected and sectioned. The mice lung was fixed by bouin's fixation solution and the visible metastasis nodules were counted. Xenograft tumor and lung section were stained with H&E. For MDA-MB-231 experimental metastasis model, $5x10^6$ MDA-MB-231 cells were injected into 6 weeks nu/nu mice (27). Lung metastases were allowed to develop for 4 months. Lung tissues collected at necropsy were formalin-fixed, paraffin-embedded, serially sectioned (4 μm), stained with hematoxylin and evaluated by microscopy to identify regions of metastatic involvement. The animal study was approved by the Institutional Animal Care and Use Committee (IACUC) from Northwestern University.

Statistical analysis

Statistical analysis was performed using two-tailed, two independent or paired sample t-tests, one-way ANOVA tests depending on the number of groups with SPSS17.0 (SPSS, Chicago, IL) (18).

RESULTS

Identification of EIF3H as a potent factor that promotes tumor invasion based on an unbiased screening

To systematically determine the impact of members of the DUB family on oncogenesis, we have recently evaluated approximately 100 DUBs in promoting tumor initiation as well as invasion, using breast cancer as a model. As shown in Figure 1A, we have initially established stable breast cancer cell lines that express members of the DUB family, and further tested the role for individual DUBs in promoting tumor invasion using a transwell invasion assay (28). Our endeavor has led to the identification of several DUBs that can promote breast tumor cell invasion with EIF3H to be the most potent (Fig. 1A).

To confirm the role of EIF3H in tumor invasion, we have extended our initial observation and further performed a variety of tumor invasion analyses such as wound healing, EMT, as well as anchorage-independent growth assays (Fig. 1B–F and Fig. S1A–J). We observed, while the elevation of EIF3H drastically increases the tumor invasion in various breast cancer cell lines, including MDA-MB-231, 4T1, depletion of EIF3H by RNA interference largely attenuates tumor invasion (Fig. 1B–F & Fig. S1A–C). Furthermore, we found that EIF3H expression correlates well with wound healing rates, indicating its role involving in cell motility (Fig. S1D–F). EMT is thought to be important in enhancing cellular mobility, invasion and resistance to apoptotic stimuli (29). We observed that disruption of EIF3H by RNA interference results in attenuation of EMT as indicated by upregulation of E-cadherin and suppression of vimentin as well as fibronectin, while elevation of EIF3H significantly enhances EMT phenotypes in breast cancer cells with dramatic alteration of morphology, loss of E-cadherin and accumulation of vimentin as well as fibronectin (Fig. S1G–J). Taken together, we have identified an unknown function for EIF3H as a potent player in promoting tumor invasion.

Abnormal accumulation of EIF3H correlates with breast cancer poor prognosis

To examine the possible clinical relevance of EIF3H in breast cancer development, we measured the protein expression levels of EIF3H in various types of breast cancer cells as well as human breast tumor tissues in comparison to adjacent normal tissues (18,26). As shown in Figure 1G, significant accumulation of EIF3H is detected in triple-negative breast cancer cell lines, including MDA-MB-231, MDA-MB-468, HCC1937, HCC38, as well as MDA-MB-231 derived cell lines such as bone metastasis 231-BoM-1833 (BoM-1833), brain metastasis 231-BrM2-831 (BrM2-831) and lung metastasis 231-LM2-4175 (LM2-4175), while relative lower EIF3H expression levels are observed in mammary epithelial cells such as 184-B5, MCF10A and MCF12A. Moderate EIF3H levels are measured in HER2 positive breast cancer cells SKBR3 and BT474. Moreover, elevated EIF3H levels are also detected in the hydroxytamoxifen-resistant cell lines MCF7-HTR, which has acquired invasive

capability in comparison to MCF7 (30,31). Meanwhile, the results from TCGA data mining further indicates that EIF3H is broadly amplified (13% to 44%) based on 6 of 7 breast cancer datasets that contain copy number analysis (CNA) data (Fig. 1H).

Furthermore, tissue arrays of 268 breast invasive ductal carcinoma and 22 adjacent normal tissue specimens were examined by IHC with anti-EIF3H and visualized by DAB staining. As shown in Figure 1I & J and Figure S2A& B, the EIF3H protein levels are significantly higher in breast tumor tissues than those in the adjacent normal tissues. Moreover, EIF3H is also accumulated in stage III, moderate-poor differentiation, and lymph node metastasis-positive patient samples (Fig. 1K–M). In addition, Kaplan-Meier survival assays for EIF3H based on TCGA database further indicate that patients with elevated EIF3H levels correlate with short relapse-free survival (RFS) times compared to patients with low EIF3H in either overall breast cancer patients, basal-type breast cancer or triple-negative breast cancer patients (Fig. 1N & O and Fig. S2C). Thus, abnormal accumulation of EIF3H levels in breast cancer tissues is associated with poor prognosis.

Discovery of uncharacterized deubiquitinating enzyme activity of EIF3H

EIF3H is classified as a member of the JAMM family of DUBs as it harbors a putative, but non-canonical, metalloprotease motif critical in coordinating a metal ion, potentially rendering isopeptidase catalytic ability (Fig. 2A) (32,33). In general, traditional metalloproteases contain a zinc ion coordinated by two histidine residues, an aspartate or a glutamate, and a water molecule. The water molecule is held by hydrogen bonding with a different glutamate residue from the second coordination sphere, in addition to the metal ion, and acts as the nucleophile during the hydrolysis reaction (34,35). While the deubiquitylation activity for most of the members in the JAMM family has been determined, whether EIF3H has isopeptidase activity to remove ubiquitin conjugates has not been reported yet because EIF3H does not have the complete metalloprotease motif in comparison with that previously reported for other JAMM members such as Rpn11, CSN5, AMSH and AMSH-LP (Fig. 2B) (36). Nevertheless, the recent demonstration of deubiquitinating enzymatic activity for EIF3F, another JAMM family member with a unique metalloprotease motif, encourages us to reconsider the current paradigm of metalloprotease motif for JAMM family and determine if EIF3H possesses isopeptidase activity (Fig. 2B) (35).

To this end, we initially carried out structural modelling analysis and simulated possible catalytic pocket based on EIF3H's non-canonical metalloprotease motif. As shown in Figure 2C, our molecular modeling analysis has revealed the role of a catalytic core for EIF3H in harboring a zinc ion and possibly executing metalloprotease activity, although EIF3H does not bear the traditional histidine residues found in the canonical JAMM motif. Our molecular dynamics (MD) simulations further suggested that the zinc ion is able to form a stable coordination (40 ns-long MD simulations) with three residues, Asp90, Asp91 and Gln121, in the EIF3H metalloprotease domain (or MPN/JAMM domain, composed of five β-strands sandwiched between α-helices; see Fig. 2C, *left*). This domain sequence is conserved from *S. pombe* to human (Fig. 2D). We further conducted druggability simulations with the DruGUI package highlighted the JAMM pocket as the most probable

among possible binding sites (*blue spheres*) with zinc ion coordinated (37). The above result suggests that the complexation of EIF3H with EIF3F further supports the binding of the zinc ion to the same site (19) (Fig. 2E). Additional residues were suggested to potentially consolidate the coordination of the metal ion since these occupied positions similar to those of residues in coordinating the zinc ion in structural homologs and were relatively conserved among orthologues (Fig. 2F).

To biochemically characterize the deubiquitinating enzyme activity for EIF3H, we subsequently conducted an *in vitro* deubiquitylation analysis using the Lys48-/Lys63-linked tetra-ubiquitin cleavage assays (38). To our surprise, results from the deubiquitylation assay demonstrates potent activity for EIF3H in cleaving Lys48-/Lys63-linked tetra-ubiquitin chain (Fig. 2G &H and Fig. S3A & B), while mutation of three residues Asp90, Asp91 and Gln121 to alanine (DDQ-AAA) in the EIF3H metalloprotease domain attenuates its activity in cleaving ubiquitin chain, suggesting that the EIF3H is a potent deubiquitinase (Fig. 2G & H).

Identification of YAP as a putative substrate for EIF3H

To search for EIF3H substrate(s) that facilitate the EIF3H-mediated breast cancer invasion, we have purified an EIF3H complex and resolved the binding partners utilizing mass spectrometry (18,39). This effort led to the identification of a series of EIF3H-binding partners, including YAP1, UBB and eIF3 subunits (EIF3A-G) (Fig. 3A & B and Table S1). The interaction between EIF3H and YAP was further validated both in endogenous and ectopically as well as *in vitro* GST/His pull-down assay (Fig. 3C & D and S4).

The identification of an interaction between EIF3H and YAP brings us a puzzle because EIF3H was previously thought as a member of the eIF3 complex involved in regulating protein translational initiation and elongation (32). To explore this mystery, we have performed an OptiPrep density gradient assay (5%-50%) based on MDA-MB-231 cell lysates. As shown in Figure 3E, we observed two peaks for EIF3H during 24 fractions. We further observed, while EIF3H cofractionated with EIF3A in peak I (Fraction 2-4), EIF3H cofractionated with YAP in peak II (Fraction 8-12), suggesting the presence of two endogenous EIF3H complexes, one eIF3 complex and another EIF3H-YAP complex. The co-IP experiments further confirmed the presence of EIF3H-YAP complex *in vivo* (Fig. 3F). To know the cellular compartmentation for EIF3H and YAP, we have performed cytoplasmic/nuclear fraction and immune-staining of EIF3H and YAP in the breast cancer cell, given YAP is a cytoplasmic and nuclear shuttle protein (10). As shown in Figure 3G–H and Figure S5A&B, both EIF3H and YAP were localized and co-immunoprecipitated in both cytosol and nucleus. In addition, the interaction between endogenous EIF3H and YAP in both cytosol and nucleus was further confirmed by confocal immunofluorescence and *in situ* Proximity Ligation Assay (Fig. 3I and S5A). Finally, the co-localization of EIF3H and YAP in the cytosol and the nucleus was demonstrated by fraction-based co-immunoprecipitation assay (Fig. S5B). Knockdown EIF3H by siRNA led to decreased YAP level in both cytosol and the nucleus, while overexpression of EIF3H resulted in elevated YAP abundance in both cytosol and nucleus (Fig. 3G and Fig. S3C-G). Altogether, our

identification of the interaction between EIF3H and YAP followed by characterization suggests that YAP is a substrate for EIF3H.

EIF3H is a *bona fide* deubiquitinase that prevents YAP from ubiquitin-dependent degradation

To further determine whether YAP is a physiologically relevant substrate for EIF3H that mediates EIF3H-promoted tumor cell invasion, we have characterized catalytic function for EIF3H in regulating YAP abundance, YAP turnover rate and YAP ubiquitylation. As shown in Figure 4A–C and Figure S5C–F, we observed that knockdown EIF3H in MDA-MB-231 and 4T1 led to a significant downregulation of YAP expression, while no alteration in YAP mRNA level and YAP cytosol/nuclear ratios were observed (Fig. 4C and Fig. S5C–F). Meanwhile, knockdown EIF3F, which directly binds to EIF3H and could function as deubiquitinase, has no effect on YAP expression and cytosol/nuclear ratios (Fig. 4A–C and Fig. S5F). Moreover, overexpressed EIF3H in MCF10A enhances YAP nuclear accumulation as well as total protein expression (Fig. S5G). We further observed that, while depletion of EIF3H results in accelerated turnover rate for YAP (Fig. 4D & E and Fig. S5H–I), elevation of EIF3H led to protection of YAP from β-TRCP/SCF-mediated YAP degradation (Fig. 4F and Fig. S5J–K) and extended the YAP half-life (Fig. 4G–H). In twelve mammary epithelial and breast cancer cell lines, EIF3H expression positively correlated with YAP expression ($R = 0.5633$, $p = 0.0565$) (Fig. S5L & M). Furthermore, we have measured YAP ubiquitylation and demonstrated that the endogenous YAP is ubiquitylated, which is tightly regulated in response to EIF3H elevation and depletion. EIF3H knockdown leads to decrease of YAP protein expression and increases ubiquitination, especially the K48-linkage specific polyubiquitination (Fig. 4I and Fig. S6A). Meanwhile, knockdown β-TRCP decrease YAP protein poly-ubiquitination in EIF3H knockdown cells, which indicated the β-TRCP is responsible for the YAP ubiquitination after EIF3H depletion (Fig. S6B). Mutation of the catalytic core of EIF3H ($EIF3H^{DDQ/AAA}$) leads to EIF3H inactive and abrogates the protective effect of YAP expression and ubiquitination from β-TRCP/SCF (Fig. 4J). Taken together, the above results suggest that EIF3H is a *bona fide* deubiquitinase preventing YAP from ubiquitin-dependent degradation.

Identification of molecular motifs on EIF3H and YAP that mediate deubiquitylation of YAP by EIF3H

For an in-depth exploration of the mechanism of recognition of YAP by the deubiquitinating enzyme EIF3H, we have next identified the molecular motifs on EIF3H as well as YAP that facilitate their interaction (18). To this aim, a series of deletion mutants for both EIF3H and YAP were engineered as illustrated in Figure 5A and C. Co-transfection of expression vectors coupled with co-immunoprecipitation leads to an initial assessment of the binding region between EIF3H and YAP (18). As shown in Figure 5B, the mapping result indicates that the amino acid stretches 34-146 on the N-terminus of EIF3H is critical in realizing its interaction with YAP. As to YAP, the initial mapping narrowed down the amino acids 1- 49 on YAP that contributes to its interaction with EIF3H (Fig. 5D). The fine mapping further demonstrated the N-terminal region of 14 amino acids on YAP as the minimum amino acid stretch that facilitates its interaction with EIF3H (Fig. 5E–G). The results from co-IP and protein degradation assays further confirmed the critical role of amino acids 1-14 at the N-

terminus of YAP in its recognition by deubiquitinase EIF3H, thereby for its stabilization (Fig. 5H).

Tryptophan 119 and Tyrosine 140 on EIF3H are critical to ensuring deubiquitylation of YAP by EIF3H

The above analysis has indicated the importance of the N-terminal 14 amino acids on YAP and the amino acid stretch 34-146 on EIF3H in mediating the interaction between YAP and EIF3H. To further identify the pivotal amino acid residues in EIF3H responsible for recognition of YAP by EIF3H, we have further performed molecular docking simulations by homology modelling service iTASSER and Haddock (40–42). Our results indicate that the amino acids 1-14 on YAP are engaged in close interactions with the EIF3H pocket featuring residues W119 and Y140 (Fig. 5I & J and Fig. S7A–F). The latter two residues have been identified as potentially important for recognition since aromatic clusters are usually found at proline-rich motif (PRMs) binding sites (43).

To determine the impact of W119 and Y140 on EIF3H in mediating the interaction between EIF3H with YAP, we have engineered double point mutant EIF3H constructs replacing by alanine (W119A and Y140A), and further tested the impact of these point mutations of EIF3H on altering the ubiquitylation and degradation of the substrate YAP. As shown in Figure 5K–M, replacement of Trp119, Tyr140 alone or combine by alanines significantly destabilized EIF3H-binding to YAP, presumably due to the perturbation of the interfacial interactions between EIF3H and YAP (Fig. 5K), and reduced the deubiquitylation capacity of EIF3H, which function same as the catalytic core mutant $EIF3H^{DDQ/AAA}$ (Fig. 5L). β-TRCP/SCF-driven YAP poly-ubiquitin conjugates were only removed by wild-type EIF3H but not the mutant $EIF3H^{YW/AA}$ and $EIF3H^{DDQ/AAA}$ (Fig. 5L). To further confirm the critical role of Trp119 and Tyr140 on EIF3H-mediated deubiquitylation of YAP, we carried out an *in vitro* deubiquitination assay. FLAG-YAP was purified and incubated with purified GST-WT or mutant EIF3H ($EIF3H^{YW/AA}$ and $EIF3H^{DDQ/AAA}$). As shown in Figure 5M and S8A & B, only the GST tagged WT EIF3H but not mutant EIF3H ($EIF3H^{YW/AA}$ and $EIF3H^{DDQ/AAA}$) could remove the poly-ubiquitin chain conjugated with YAP. Thus, Trp119 and Tyr140 on EIF3H are critical to ensuring the EIF3H-mediated removal of YAP poly-ubiquitin conjugates.

The results from the previous mapping and molecular docking analyses demonstrated the importance of the N-terminal fourteen residues on YAP contributing to its interaction with EIF3H (Fig. 5E–J). Our blast analysis further suggests the potential role for the four conserved proline residues in this region that facilitate the interaction between YAP and EIF3H (Fig. 5N). To test the importance of these four prolines residues, we have constructed a YAP mutant with replacing four prolines residues by alanine. As shown in Figure 5O, replacement of four proline residues (YAP^{4PA}) significantly reduced its binding capacity with EIF3H. In addition, while EIF3H can remove β-TRCP/SCF-mediated poly-ubiquitin conjugates from wild-type YAP, it fails to remove ubiquitin chain from prolines mutated YAP (Fig. 5P).

Mutated EIF3H catalytic core or disrupted EIF3H-YAP binding affect YAP expression independent on translation

As one of the members of the eIF3 complex, EIF3H has been reported to control a series of mRNA translation, such as ENO2, TIMP1 (44,45). Therefore, we further explore whether YAP is also the specific translational targets for EIF3H. We first established EIF3H knockdown cells and then added back the wildtype and mutant EIF3H ($EIF3H^{DDQ/AAA}$ and $EIF3H^{YW/AA}$) and found that knockdown EIF3H could decrease YAP, ENO2 and CTGF expression, add back wildtype EIF3H could recover all these proteins expression in MDA-MB-231 and MDA-MB-468 cells (Fig. 6A). However, add back the mutant EIF3H ($EIF3H^{DDQ/AAA}$ and $EIF3H^{YW/AA}$) could only recovery ENO2 but not YAP and CTGF expression (Fig. 6A). Meanwhile, in cell proliferation and transwell assay, while both wildtype and mutant EIF3H all fully recover cell proliferation (Fig. 6B & C), the mutant EIF3H failed to fully recover the cell transwell invasion as the wildtype EIF3H (Fig. 6D–F). To avoid the cell proliferation effect on transwell invasion, we also include the mitomycin C as a control, which could abrogate cell proliferation but no effect on cell invasion (Fig. 6D–F). The mutant EIF3H ($EIF3H^{DDQ/AAA}$ and $EIF3H^{YW/AA}$) also lose the effects that promote YAP expression and epithelial-mesenchymal transition when staining of YAP, E-cadherin and Fibronectin (FN) in MCF10A cells (Fig. S8C). Further luciferase activity assay of YAP activity reporter, HIP (Hippo-YAP signaling incompetent promoter; negative control)-flash and HOP (Hippo-YAP signaling optimal promoter)-flash reporters, indicated that the mutant EIF3H ($EIF3H^{DDQ/AAA}$ and $EIF3H^{YW/AA}$) failed to restore the YAP activity (Fig. 6G). To further dissect whether EIF3H mutant affects YAP mRNA binds to eIF3 complex, the wildtype or mutant tagged EIF3H were immunoprecipitated with FLAG-tagged and their binding mRNA were quantified by qPCR. Intersecting, all three mRNA, YAP, ENO2 and TIMP1 mRNA could be pulldown by FLAG-tagged EIF3H, mutation of EIF3H has no effect on mRNA pull-down (Fig. 6H). To investigate the mutation of EIF3H on the eIF3 complex, we further applied the OptiPrep density gradient assay (5%−30%). Interesting, the wildtype EIF3H has two peeks (peak I and II) accumulation as the endogenous EIF3H (Fig. 3E), the mutant EIF3H has only one major peak (peak II). Meanwhile, immunoprecipitation of wildtype or mutant EIF3H in fraction 4 (peak I) and 10 (peak II) further implicated that the YAP proteins only co-IP with wildtype EIF3H in fraction 4 (peak I) (Fig. 6I). The inclusion of wildtype or mutant EIF3H in the eIF3 complex has no difference when blotting with EIF3A after EIF3H immunoprecipitated in peak II (Fig. 6J). These results implicated that mutated EIF3H catalytic core ($EIF3H^{DDQ/AAA}$) or disrupted EIF3H-YAP binding ($EIF3H^{YW/AA}$) has no effect on eIF3 complex integrity, YAP mRNA binds to eIF3 complex. We also used MG132 to treat MDA-MB-231- ShEIF3H-1# and control cells, and interesting found that long-term treatment of MG132 could reach to equal YAP protein accumulation in both cell lines, which implicated that the translation of YAP mRNA has not been disturbed by the loss of EIF3H (Fig. 6K). Therefore, we conclude that EIF3H control YAP expression is major depend on the ubiquitin-proteasome system but not translation.

Stabilization of YAP by EIF3H promotes breast cancer invasion and metastasis

YAP was previously demonstrated to be a pivotal oncogenic factor in promoting cell proliferation, migration, and invasion (1,11). We next asked what the physiological consequence of YAP stabilization by abnormal EIF3H function is on tumor invasion. We

further attempted to address the effect on the upstream signaling that participate to modulate the EIF3H-YAP cascade in cancer status. In addition, we anticipated to determining the clinical relevance for dysregulated EIF3H-YAP axis in breast tumor the lung metastasis using human breast cancer mouse metastasis model.

To further determine the impact of EIF3H in stabilizing YAP and promoting YAP-mediated transcriptional activity, we examined the effect of elevated EIF3H on the alteration of YAP function using a transwell assay. As shown in Figure 7A–D and S9A–C, knockdown of either the YAP and CTGF expression abrogated EIF3H-driven tumor cell invasion. In addition, replacement of four conserved proline residues on YAP (YAP^{4PA}) disrupts its binding to EIF3H that in turn leads to the reduction of YAP substrate reporter activity and YAP-driven breast tumor cell invasion (Fig. 7E & F and S9D & E). Meanwhile, there is no difference in transwell invasion assay between overexpression of mutant and wildtype YAP in MDA-MB-231 cells with EIF3H knockdown, which indicated the difference of YAP^{WT} and YAP^{4PA} is dependent on EIF3H protein (Fig. S9F & G).

The previous report demonstrated EIF3H is regulated in response to mTOR-S6K1 cascade, where EIF3H can be phosphorylated by S6K1 kinase through the serine 183 on EIF3H (25). Moreover, upstream signaling by growth factors or GPCRs has been linked to regulation of YAP stability (46,47). Thus, we asked whether these signals play a role in regulating the EIF3H-YAP axis. To answer this question, we employed a pharmacological approach to determine the involvement of the upstream signaling. As shown in Figure 7G and Figure S10A–D, we found that the inhibitors for PI3K (LY294002), S6K1 (PF4708671), Src (dasatinib) and mTOR (rapamycin) block EIF3H Ser/Thr phosphorylation, EIF3H-YAP binding and EIF3H-governed YAP accumulation but no effect for EIF3H/EIF3A binding. Intriguingly, we observed that the replacement of serine 183 by alanine on EIF3H significantly decreases EIF3H-mediated YAP accumulation (Fig. 7H and Fig. S10D). Blockade of S6K1 or mTOR cascade by S6K1 inhibitor (PF4708671) or mTOR inhibitor (rapamycin) attenuates colocalization of EIF3H with YAP indicated by an *in situ* Proximity Ligation Assay (Fig. S10E). Finally, we observed that inhibitor for PI3K, S6K1, Src and mTOR sensitizes verteporfin, a YAP-TEAD inhibitor (48) in suppressing tumor cell proliferation and transwell invasion (Fig. 7I and Fig. S10F & G).

To further determine the clinical relevance for dysregulated EIF3H-YAP axis in breast tumor lung metastasis, we have utilized both mouse and human breast cancer mouse metastasis models (27). Based on the mouse 4T1 breast cancer spontaneous metastasis model, $5x10^5$ 4T1 cells with stable expression of ShEIF3H, ShEIF3H/$EIF3H^{WT}$ or ShEIF3H/ $EIF3H^{YW/AA}$ expression were planted to the Balb/c mice mammary fat pad. We observed that loss of EIF3H in 4T1 cells led to decreased YAP and ENO2 expression. Add-back wildtypeEIF3H could recover YAP and ENO2 expression, while the mutant EIF3H failed to recover YAP expression (Fig. S11A). In the primary tumor growth, while the loss of EIF3H decrease cell proliferation and tumor growth, overexpression of both wild-type and mutant EIF3H resulted in full recovery of tumor growth suggesting a minor effect of EIF3H-YAP on tumor growth (Fig. 7J–L and Fig. S11B–E). In the spontaneous lung metastasis model, we observed that loss of EIF3H significantly decreased lung metastasis nodules. To our surprise, we observed, while only overexpression of the wild-type EIF3H fully recapitulates lung

metastasis, the expression of mutant EIF3H fails to restore lung metastasis, indicating that EIF3H-YAP axis is critical for EIF3H-driven tumor invasion and metastasis (Fig. 7M and Fig. S11F). In addition to the 4T1 mouse metastasis model, we have also tested the effect of EIF3H in human breast cancer experimental metastasis xenograft model (27). 5×10^5 MDA-MB-231 cells with stable expression of ShEIF3H, ShEIF3H/EIF3H^{WT}, ShEIF3H/EIF3H$^{DDQ/AAA}$ or ShEIF3H/EIF3H$^{YW/AA}$ were injected through tail vein into 6 weeks nu/nu mice. Mice were sacrificed 4 months later and the collected lungs were sectioned for staining with H/E as well as counting micrometastasis foci. As shown in Figure 7N & O, we observed that lung metastasis of MDA-MB-231 was recovered by add-back of EIF3H^{WT}, but not EIF3H$^{DDQ/AAA}$ and EIF3H$^{YW/AA}$. Collectively, the results from various lines strongly suggest that the stabilization of YAP due to deregulated EIF3H is a crucial causal factor in promoting tumor invasion and distant metastasis (Fig. 7P).

DISCUSSION

Our unbiased screening led to the identification of an undocumented deubiquitinase function for EIF3H in promoting breast tumor metastasis, which raises two new questions: (1) how does EIF3H achieve its deubiquitinase enzymatic activity due to its lack of histidine residues to form a catalytic triad, and (2) how does EIF3H perform its previously documented role in regulating protein translation and it's the newly identified role in governing YAP stability (32). To resolve the mechanism of how EIF3H acts as a deubiquitinase without histidine residues in the catalytic triad, we conducted 3D molecular dynamic studies coupled with a series of mutagenesis and biochemical characterization (35). Our 3D modeling study followed by comprehensive characterizations have resulted in a new finding that, instead of traditional histidine residues, aspartic acids 90, 91 and glutamine 121 on EIF3H coordinate a zinc ion that in turn satisfies the catalytic triad in orchestrating EIF3H enzymatic activity. This finding complements with the previous report by the Brou group that EIF3F, without conventional MPN sequence, executes isopeptidase activity by utilizing a distal histidine residue to form a metal catalytic triad (35). Results from biochemical characterization have further revealed that EIF3H forms two distinct complexes with either eIF3 or YAP, respectively, which explains EIF3H's dual functions of translation regulation and modulation of Hippo-YAP-mediated tumor metastasis (1,35). Our work for the first time unveils an unexpected catalytic role for EIF3H as a deubiquitinase that dictates Hippo pathway-mediated invasion and metastasis by stabilizing YAP, which provides a potential novel target to control tumor metastasis.

EIF3H was reported as a subunit of eIF3 complex, which regulated processes of initiation and elongation during protein translation (19). Subunits such as eIF3H, eIF3F (from eIF3 complex), CSN5 (from COP9 signalosome) and Rpn11 (from 19S proteasome) harbor consensus of MPN motifs that could have metalloprotease function (49). Identification of deubiquitinase enzymatic activity for EIF3H led us to ask how EIF3H confers its role in regulating protein translation and governing YAP stabilization. Possibly, EIF3H could exist by itself or forms various complexes in order to conduct different functions, which is supported by results from our OptiPrep density gradient protein fractionation assay. In the fractionation analysis, we observed the presence of two peaks for EIF3H, one associating with EIF3A and another cofractioning with YAP. The presence of multiple EIF3H peaks in

density fractionations suggests, possibly like CSN5 in COP9 signalosome as well as Rpn11 in the 19S proteasome, EIF3H executes versatile cellular functions through forming various protein complexes. Future knock-in mouse genetic study by intercepting the binding between EIF3H and YAP or muting EIF3H deubiquitinase activity could specifically address the different impact of EIF3H in regulating Hippo-YAP pathway and EIF3H in translation initiation pathway in mice development, tumorigenesis as well as metastasis.

Retention of transcriptional factor YAP in the cytosol by activated Hippo signaling leads to growth inhibition, whereas translocation of YAP from the cytosol into nucleus due to its dephosphorylation results in transcription of a set of oncogenic genes that in turn enhance growth and tumorigenesis (2,50). In the presence of Hippo signaling, phosphorylation of YAP and 14-3-3-mediated cytoplasmic sequestration maintains YAP localization in the cytosol, therefore the cytoplasmic YAP could be ubiquitylated by β-TRCP-SCF ubiquitin E3 ligase leading to degradation (4,6). Other than the translation-initiation function of EIF3H, in the present study, our finding that EIF3H promotes metastasis through stabilizing YAP addresses a knowledge gap for YAP turnover regulation. We show that while β-TRCP-SCF complex suppresses YAP protein levels, removal of ubiquitin chain from YAP by EIF3H counteracts β-TRCP-SCF-mediated YAP ubiquitylation, thereby resulting in YAP stabilization. Our results further imply that EIF3H could be a crucial signaling node that mediates crosstalk between Hippo signaling with other oncogenic pathways since EIF3H enhanced stabilization of YAP and tumorigenesis can be attenuated by PI3K, S6K1, Src and mTOR inhibitors. Given the impact of Hippo-YAP pathway in the regulation of cell proliferation, tumorigenesis, cancer stem cell self-renewal, chemoresistance, and metastasis, our finding of new function for EIF3H in the stabilization of YAP that in turn promotes tumor invasion and metastasis could provide a novel targeting strategy for anti-cancer treatment (1,2).

Supplementary Material

Refer to Web version on PubMed Central for supplementary material.

ACKNOWLEDGMENTS

This work was supported by the Northwestern University Zell scholar fund and grants from the National Institutes of Health (R01CA154695). Support from National Nature Science Foundation of China (81130043) is acknowledged by ZL. Support from NIH grants U54 HG008540 and P41 GM103712 is gratefully acknowledged by IB.

We are grateful to Drs. Wade Harper and Jianping Jin for kindly providing the TAP purification vector. We appreciate the proteomic core at the University of Pittsburgh for mass spectrometry analyses. We thank all members of Wan, Liu and Bahar laboratories for their helpful discussion.

REFERENCE

1. Lamar JM, Stern P, Liu H, Schindler JW, Jiang ZG, Hynes RO. The Hippo pathway target, YAP, promotes metastasis through its TEAD-interaction domain. Proceedings of the National Academy of Sciences of the United States of America 2012;109:E2441–50 [PubMed: 22891335]
2. Moroishi T, Park HW, Qin B, Chen Q, Meng Z, Plouffe SW, et al. A YAP/TAZ-induced feedback mechanism regulates Hippo pathway homeostasis. Genes & development 2015;29:1271–84 [PubMed: 26109050]

3. Moroishi T, Hayashi T, Pan WW, Fujita Y, Holt MV, Qin J, et al. The Hippo Pathway Kinases LATS1/2 Suppress Cancer Immunity. Cell 2016;167:1525–39 e17 [PubMed: 27912060]
4. Zhao B, Li L, Tumaneng K, Wang CY, Guan KL. A coordinated phosphorylation by Lats and CK1 regulates YAP stability through SCF(beta-TRCP). Genes & development 2010;24:72–85 [PubMed: 20048001]
5. Kim Y, Kim W, Song Y, Kim JR, Cho K, Moon H, et al. Deubiquitinase YOD1 potentiates YAP/TAZ activities through enhancing ITCH stability. Proceedings of the National Academy of Sciences of the United States of America 2017;114:4691–6 [PubMed: 28416659]
6. He M, Zhou Z, Shah AA, Hong Y, Chen Q, Wan Y. New insights into posttranslational modifications of Hippo pathway in carcinogenesis and therapeutics. Cell division 2016;11:4 [PubMed: 27042197]
7. Tu K, Yang W, Li C, Zheng X, Lu Z, Guo C, et al. Fbxw7 is an independent prognostic marker and induces apoptosis and growth arrest by regulating YAP abundance in hepatocellular carcinoma. Mol Cancer 2014;13:110 [PubMed: 24884509]
8. Li W, Cooper J, Zhou L, Yang C, Erdjument-Bromage H, Zagzag D, et al. Merlin/NF2 loss-driven tumorigenesis linked to CRL4(DCAF1)-mediated inhibition of the hippo pathway kinases Lats1 and 2 in the nucleus. Cancer cell 2014;26:48–60 [PubMed: 25026211]
9. Ma B, Chen Y, Chen L, Cheng H, Mu C, Li J, et al. Hypoxia regulates Hippo signalling through the SIAH2 ubiquitin E3 ligase. Nature cell biology 2015;17:95–103 [PubMed: 25438054]
10. Yu FX, Guan KL. The Hippo pathway: regulators and regulations. Genes & development 2013;27:355–71 [PubMed: 23431053]
11. Pan D The hippo signaling pathway in development and cancer. Dev Cell 2010;19:491–505 [PubMed: 20951342]
12. Toloczko A, Guo F, Yuen HF, Wen Q, Wood SA, Ong YS, et al. Deubiquitinating Enzyme USP9X Suppresses Tumor Growth via LATS Kinase and Core Components of the Hippo Pathway. Cancer Res 2017;77:4921–33 [PubMed: 28720576]
13. He M, Zhou Z, Wu G, Chen Q, Wan Y. Emerging role of DUBs in tumor metastasis and apoptosis: Therapeutic implication. Pharmacology & therapeutics 2017;177:96–107 [PubMed: 28279784]
14. Abdul Rehman SA, Kristariyanto YA, Choi SY, Nkosi PJ, Weidlich S, Labib K, et al. MINDY-1 Is a Member of an Evolutionarily Conserved and Structurally Distinct New Family of Deubiquitinating Enzymes. Molecular cell 2016;63:146–55 [PubMed: 27292798]
15. Ronau JA, Beckmann JF, Hochstrasser M. Substrate specificity of the ubiquitin and Ubl proteases. Cell research 2016;26:441–56 [PubMed: 27012468]
16. Wang B, Jie Z, Joo D, Ordureau A, Liu P, Gan W, et al. TRAF2 and OTUD7B govern a ubiquitin-dependent switch that regulates mTORC2 signalling. Nature 2017;545:365–9 [PubMed: 28489822]
17. Yuan J, Luo K, Zhang L, Cheville JC, Lou Z. USP10 regulates p53 localization and stability by deubiquitinating p53. Cell 2010;140:384–96 [PubMed: 20096447]
18. Zhou Z, Luo A, Shrivastava I, He M, Huang Y, Bahar I, et al. Regulation of XIAP Turnover Reveals a Role for USP11 in Promotion of Tumorigenesis. EBioMedicine 2017;15:48–61 [PubMed: 28040451]
19. des Georges A, Dhote V, Kuhn L, Hellen CU, Pestova TV, Frank J, et al. Structure of mammalian eIF3 in the context of the 43S preinitiation complex. Nature 2015;525:491–5 [PubMed: 26344199]
20. Tomlinson IP, Webb E, Carvajal-Carmona L, Broderick P, Howarth K, Pittman AM, et al. A genome-wide association study identifies colorectal cancer susceptibility loci on chromosomes 10p14 and 8q23.3. Nat Genet 2008;40:623–30 [PubMed: 18372905]
21. Cappuzzo F, Varella-Garcia M, Rossi E, Gajapathy S, Valente M, Drabkin H, et al. MYC and EIF3H Coamplification significantly improve response and survival of non-small cell lung cancer patients (NSCLC) treated with gefitinib. J Thorac Oncol 2009;4:472–8 [PubMed: 19204574]
22. Okamoto H, Yasui K, Zhao C, Arii S, Inazawa J. PTK2 and EIF3S3 genes may be amplification targets at 8q23-q24 and are associated with large hepatocellular carcinomas. Hepatology 2003;38:1242–9 [PubMed: 14578863]

23. Nupponen NN, Porkka K, Kakkola L, Tanner M, Persson K, Borg A, et al. Amplification and overexpression of p40 subunit of eukaryotic translation initiation factor 3 in breast and prostate cancer. Am J Pathol 1999;154:1777–83 [PubMed: 10362802]
24. Zhu Q, Qiao GL, Zeng XC, Li Y, Yan JJ, Duan R, et al. Elevated expression of eukaryotic translation initiation factor 3H is associated with proliferation, invasion and tumorigenicity in human hepatocellular carcinoma. Oncotarget 2016;7:49888–901 [PubMed: 27340783]
25. Zhang L, Smit-McBride Z, Pan X, Rheinhardt J, Hershey JW. An oncogenic role for the phosphorylated h-subunit of human translation initiation factor eIF3. The Journal of biological chemistry 2008;283:24047–60 [PubMed: 18544531]
26. Hu D, Gur M, Zhou Z, Gamper A, Hung MC, Fujita N, et al. Interplay between arginine methylation and ubiquitylation regulates KLF4-mediated genome stability and carcinogenesis. Nature communications 2015;6:8419
27. Minn AJ, Gupta GP, Siegel PM, Bos PD, Shu W, Giri DD, et al. Genes that mediate breast cancer metastasis to lung. Nature 2005;436:518–24 [PubMed: 16049480]
28. Kramer N, Walzl A, Unger C, Rosner M, Krupitza G, Hengstschlager M, et al. In vitro cell migration and invasion assays. Mutation research 2013;752:10–24 [PubMed: 22940039]
29. Kalluri R, Weinberg RA. The basics of epithelial-mesenchymal transition. The Journal of clinical investigation 2009;119:1420–8 [PubMed: 19487818]
30. Hiscox S, Jiang WG, Obermeier K, Taylor K, Morgan L, Burmi R, et al. Tamoxifen resistance in MCF7 cells promotes EMT-like behaviour and involves modulation of beta-catenin phosphorylation. Int J Cancer 2006;118:290–301 [PubMed: 16080193]
31. Li Y, Wu Y, Abbatiello TC, Wu WL, Kim JR, Sarkissyan M, et al. Slug contributes to cancer progression by direct regulation of ERalpha signaling pathway. Int J Oncol 2015;46:1461–72 [PubMed: 25652255]
32. Hinnebusch AG. eIF3: a versatile scaffold for translation initiation complexes. Trends in biochemical sciences 2006;31:553–62 [PubMed: 16920360]
33. Komander D, Clague MJ, Urbe S. Breaking the chains: structure and function of the deubiquitinases. Nature reviews Molecular cell biology 2009;10:550–63 [PubMed: 19626045]
34. Walden M, Masandi SK, Pawlowski K, Zeqiraj E. Pseudo-DUBs as allosteric activators and molecular scaffolds of protein complexes. Biochem Soc Trans 2018;46:453–66 [PubMed: 29472364]
35. Moretti J, Chastagner P, Gastaldello S, Heuss SF, Dirac AM, Bernards R, et al. The translation initiation factor 3f (eIF3f) exhibits a deubiquitinase activity regulating Notch activation. PLoS biology 2010;8:e1000545 [PubMed: 21124883]
36. Forster F, Unverdorben P, Sledz P, Baumeister W. Unveiling the long-held secrets of the 26S proteasome. Structure 2013;21:1551–62 [PubMed: 24010714]
37. Bakan A, Nevins N, Lakdawala AS, Bahar I. Druggability Assessment of Allosteric Proteins by Dynamics Simulations in the Presence of Probe Molecules. J Chem Theory Comput 2012;8:2435–47 [PubMed: 22798729]
38. Edelmann MJ, Iphofer A, Akutsu M, Altun M, di Gleria K, Kramer HB, et al. Structural basis and specificity of human otubain 1-mediated deubiquitination. The Biochemical journal 2009;418:379–90 [PubMed: 18954305]
39. Gamper AM, Qiao X, Kim J, Zhang L, DeSimone MC, Rathmell WK, et al. Regulation of KLF4 turnover reveals an unexpected tissue-specific role of pVHL in tumorigenesis. Mol Cell 2012;45:233–43 [PubMed: 22284679]
40. Zhang Y I-TASSER server for protein 3D structure prediction. BMC Bioinformatics 2008;9:40 [PubMed: 18215316]
41. van Zundert GCP, Rodrigues J, Trellet M, Schmitz C, Kastritis PL, Karaca E, et al. The HADDOCK2.2 Web Server: User-Friendly Integrative Modeling of Biomolecular Complexes. J Mol Biol 2016;428:720–5 [PubMed: 26410586]
42. Dominguez C, Boelens R, Bonvin AM. HADDOCK: a protein-protein docking approach based on biochemical or biophysical information. J Am Chem Soc 2003;125:1731–7 [PubMed: 12580598]

43. Ball LJ, Kuhne R, Schneider-Mergener J, Oschkinat H. Recognition of proline-rich motifs by protein-protein-interaction domains. Angew Chem Int Ed Engl 2005;44:2852–69 [PubMed: 15880548]
44. Choudhuri A, Maitra U, Evans T. Translation initiation factor eIF3h targets specific transcripts to polysomes during embryogenesis. Proceedings of the National Academy of Sciences of the United States of America 2013;110:9818–23 [PubMed: 23716667]
45. Choe J, Lin S, Zhang W, Liu Q, Wang L, Ramirez-Moya J, et al. mRNA circularization by METTL3-eIF3h enhances translation and promotes oncogenesis. Nature 2018;561:556–60 [PubMed: 30232453]
46. Fan R, Kim NG, Gumbiner BM. Regulation of Hippo pathway by mitogenic growth factors via phosphoinositide 3-kinase and phosphoinositide-dependent kinase-1. Proceedings of the National Academy of Sciences of the United States of America 2013;110:2569–74 [PubMed: 23359693]
47. Yu FX, Zhao B, Panupinthu N, Jewell JL, Lian I, Wang LH, et al. Regulation of the Hippo-YAP pathway by G-protein-coupled receptor signaling. Cell 2012;150:780–91 [PubMed: 22863277]
48. Johnson R, Halder G. The two faces of Hippo: targeting the Hippo pathway for regenerative medicine and cancer treatment. Nature reviews Drug discovery 2014;13:63–79 [PubMed: 24336504]
49. Glickman MH, Rubin DM, Coux O, Wefes I, Pfeifer G, Cjeka Z, et al. A subcomplex of the proteasome regulatory particle required for ubiquitin-conjugate degradation and related to the COP9-signalosome and eIF3. Cell 1998;94:615–23 [PubMed: 9741626]
50. Justice RW, Zilian O, Woods DF, Noll M, Bryant PJ. The Drosophila tumor suppressor gene warts encodes a homolog of human myotonic dystrophy kinase and is required for the control of cell shape and proliferation. Genes & development 1995;9:534–46 [PubMed: 7698644]

SIGNIFICANCE

This work demonstrates that EIF3H is a novel bona fide deubiquitinase that counteracts YAP ubiquitylation and proteolysis, and stabilization of YAP by EIF3H promotes tumor invasion and metastasis.

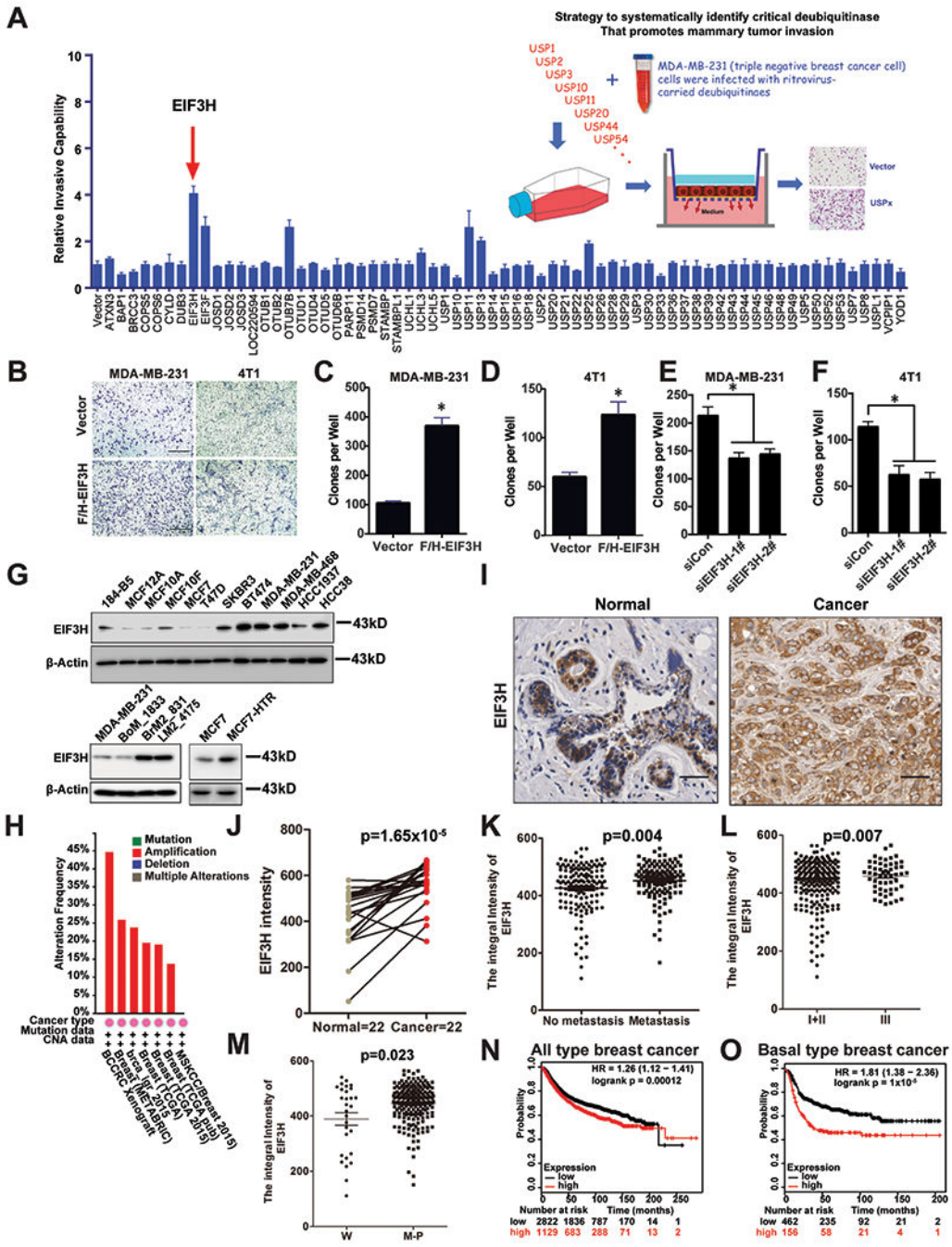

Figure 1. EIF3H promotes breast tumor cell invasion and correlates with breast cancer poor prognosis.

(**A**) Approximately 100 deubiquitinase genes carried by the retroviral vector were utilized to establish stable expression cell lines based on MDA-MB-231, respectively. The capacity of each deubiquitinase in promoting the MDA-MB-231 invasion was systematically evaluated by a transwell invasion assay. EIF3H turns to be the most potent one promotes cell invasion. (**B-D**) Validation of elevated expression of EIF3H in MDA-MB-231 (**B-C**) and 4T1 (**D**) in promoting transwell invasion. The representative crystal violet staining was shown in **B** and

the summary count of invasive cells staining was shown in **C** and **D**. Scale bars, 100μm. (**E-F**) Knockdown EIF3H in both MDA-MB-231 (**E**) and 4T1 (**F**) significantly decrease transwell invasion. The asterisk indicated statistical significance ($p<0.05$). (**G**) Expression of EIF3H in mammary gland epithelial cell and various types of breast cancer cell lines. (**H**) The mutation, amplification and deletion status of EIF3H in breast cancer in cancer genomics (http://www.cbioportal.org/). (**I, J**) Tissue arrays of 268 breast invasive ductal carcinoma and 22 pairs of primary cancer and adjacent normal tissue specimens were subjected to immunohistochemistry with anti-EIF3H staining. Representative normal and cancer tissue staining are shown in **C**. Scale bar, 50μm. (**J**) Statistical results of **I**. (**K-M**) Summary of the EIF3H staining in subgroups, including (**K**) non-lymph node metastasis (n=140) vs. lymph node metastasis (n=128); (**L**) stage I+II (n=214) vs. III (n=53); and (**M**) Well differentiation (W, n=30) vs. moderate/poor differentiation (M+P, n=209). (**N-O**) Patients with EIF3H overexpression show short relapse-free survival (RFS) time in comparison with patients with low EIF3H in either overall breast cancer (**N**) and basal type breast cancer (**O**) patients.

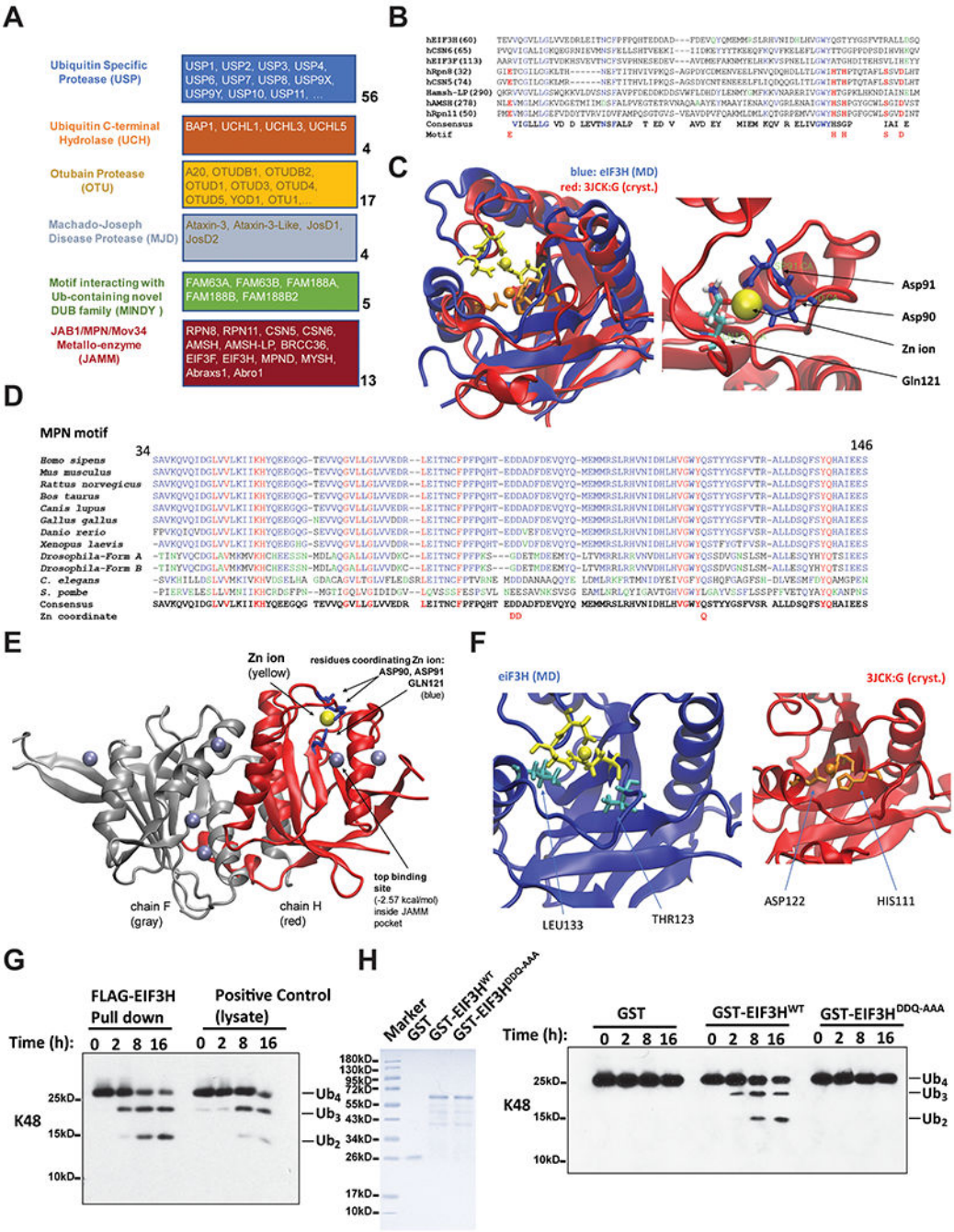

Figure 2. Discovery of uncharacterized deubiquitinating enzyme activity for EIF3H.

(**A**) Schematic classification of 100 human DUBs into five families. (**B**) Sequence alignment of JAMM family members Rpn11, AMSH, AMSH-LP and CSN5, EIF3H and EIF3F showing the consensus of two histidine residues followed by an aspartate or glutamate in the metalloprotease motif. EIF3H and EIF3F lack the conserved histidines in their putative catalytic region. (**C**) Result from structural modeling and simulation of the catalytic core (MPN domain) of EIF3H, indicating that Asp90, Asp91 and Gln121 form a catalytic triad to coordinate a Zn^{++} ion, in support of the metalloprotease activity for EIF3H. Note the close

superposition of the EIF3H MPN domain conformation stably maintained after 40 ns MD simulations (*blue*) on the ubiquitin C-terminal hydrolase RPN11 structure (*red*) (PDB id: 3JCK, chain G) resolved in the yeast 26S proteasome lid crystal structure. (**D**) Alignment of EIF3H across multiple species shows the conservation of Asp90, Asp91 and Gln121 located on the MPN domain. (**E**) Zinc coordination in the JAMM/MPN pocket of EIF3H (chain H) is observed in a simulation, where EIF3F (chain F, *gray*) has been also included, which may help in stabilizing chain H (in particular, helix 98–108 and the flexible loop containing Asp90 and Asp91), thus facilitating the coordination of zinc ion. (**F**) Hydrophobic residues (Leu133 and Thr123) were observed in MD simulations to further assist the coordination of Zn^{++} ion by the catalytic triad of EIF3H (*left*). The *right* diagram displays the same region in the hydrolase displayed in panel **C**. (**G-H**) Lys48-linked tetra-ubiquitin in-vitro cleavage assay. (**G**) *In vitro* tetra-ubiquitin (Ub4) cleavage assay for wild-type EIF3H purified from HEK293 cells (transfection with FLAG-EIF3H) and cell lysate as the positive control. (**H**) The protein of GST, GST-EIF3H^{WT} and GST-EIF3H$^{DDQ\text{-}AAA}$ were incubated with tetra-ubiquitin for the indicated time. Mutants of EIF3H failed cleave tetra-ubiquitin.

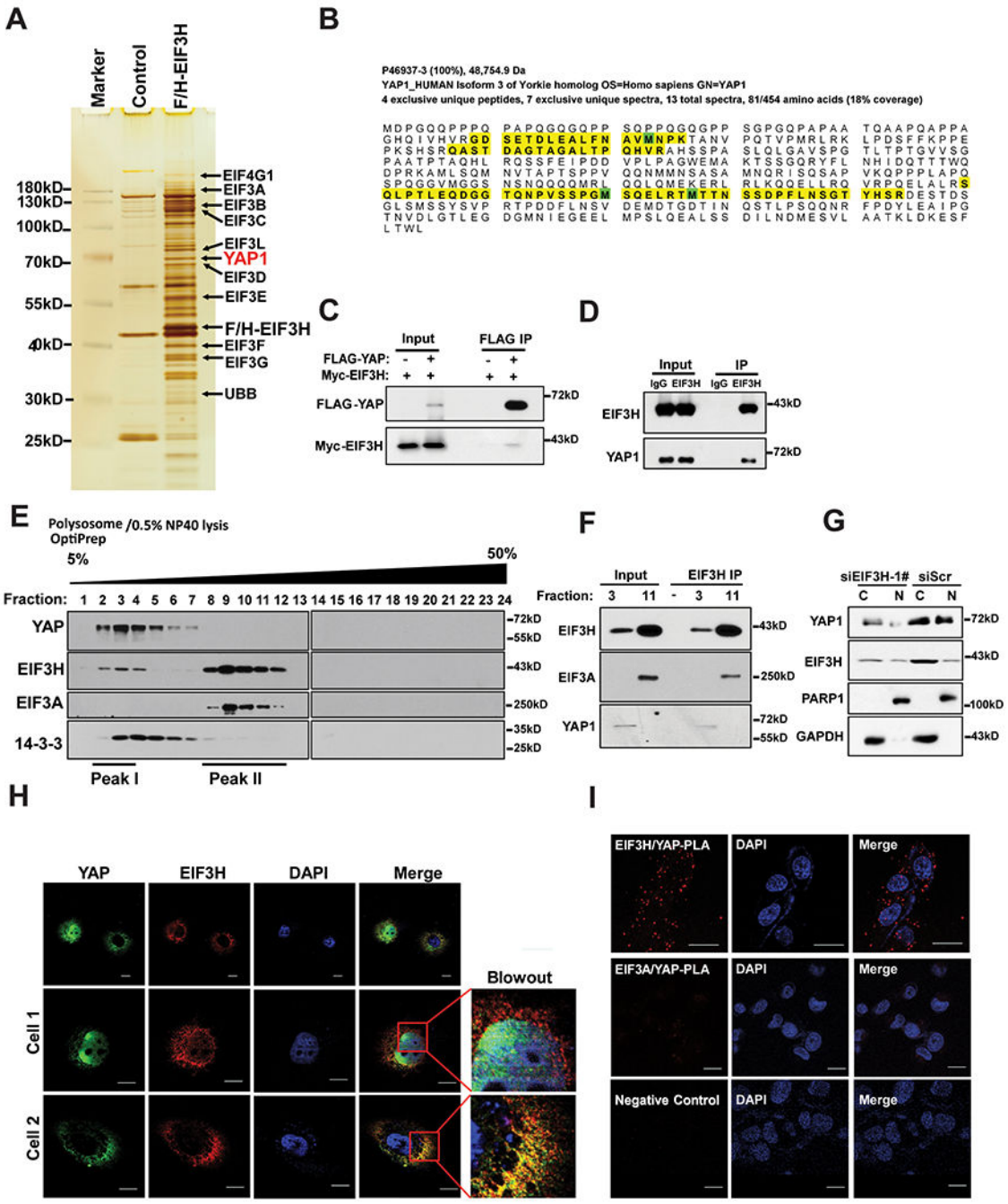

Figure 3. Identification of YAP as a binding partner of EIF3H.

(**A**) Engineering of TAP-EIF3H stable expression clone in MDA-MB-231 and purification of the EIF3H protein complex. The purified EIF3H protein complex was subjected to mass spectrometry analysis. Several proteins including YAP were found in the complex. (**B**) The sequences of mass spectrometry analysis for identification of YAP1 (P46937–3). The identified peptides were labeled in yellow. (**C**) Validation of interaction between ectopically expressed FLAG-YAP and Myc-EIF3H in 293T cells using immunoprecipitation. (**D**) Endogenous EIF3H co-immunoprecipitated with endogenous YAP in MDA-MB-231 cells.

(**E**) Endogenous EIF3H co-fractionated with YAP in OptiPrep density gradient assay (5% −50%) in MDA-MB-231 lysates. The representative subunit of EIF3 complex EIF3A and YAP binding protein 14–3-3 was measured as well. (**F**) Validation of co-fractionation and co-immunoprecipitation between EIF3H and YAP in number 3 lysate fraction and interaction of EIF3H with EIF3A in number 11 lysate fraction. (**G**) Cytosol-Nuclear fraction assay of MDA-MB-231 indicated that EIF3H exists in both cytosol (C) and nucleus (N). Knockdown EIF3H decreases both cytoplasmic and nuclear partition of YAP. (**H**) EIF3H (red) and YAP (green) are co-localized in MDA-MB-231 in both cytosol and nuclear by confocal microscopy. The blowout shows enlarged images of the dashed square. Scale bar, 5μm. (**I**) Validation of the interaction between endogenous EIF3H and YAP by *in situ* Proximity Ligation Assay (PLA). No positive staining in EIF3A/YAP or rabbit antibody (negative control)/YAP PLA assay. Scale bar, 10μm.

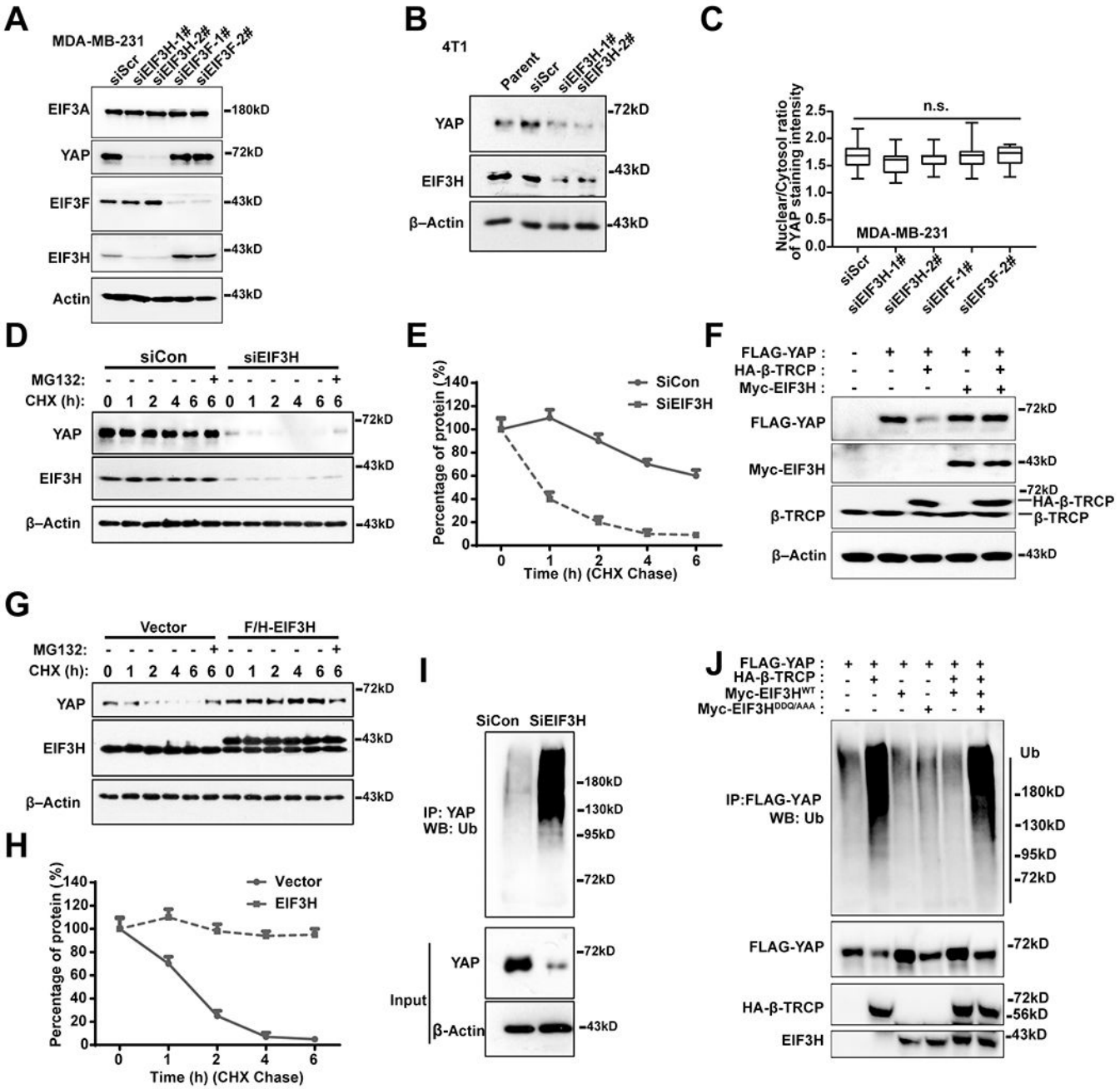

Figure 4. EIF3H acts as a deubiquitinase that stabilizes YAP from ubiquitin-dependent degradation.

(**A, B**) Knockdown EIF3H in MDA-MB-231 (**A**) and 4T1 (**B**) cells leads to decreased YAP expression. Knockdown EIF3F in MDA-MB-231 (**A**) has no effect on YAP expression. (**C**) The nuclear/cytosol ratio of YAP staining intensity in MDA-MB-231 cells after EIF3H or EIF3F knockdown. n.s., not significant. (**D, E**) Depletion of EIF3H results in a decreased turnover half-life of YAP in MDA-MB-231 cells (**D**). The density of the YAP band was quantified, normalized to the internal control β-actin, which are presented in the right panel (**E**). (**F**) Elevated expression of EIF3H blocked the β-TRCP promoted YAP degradation. (**G,**

H) Elevated expression of EIF3H leads to prolonged YAP protein turnover half-life in MCF10A. The density of the YAP band was quantified, normalized to the internal control β-actin, which are presented in the right panel (**H**). (**I**) Knockdown EIF3H increases YAP ubiquitination. MDA-MB-231 cells were transfected with EIF3H siRNA and then pull down with YAP. (**J**) Expression of wildtype EIF3H ($EIF3H^{WT}$) but not EIF3H with catalytic core mutant ($EIF3H^{DDQ/AAA}$) results in decreased YAP ubiquitin-conjugates driven by β-TRCP. HEK293T cells were transfected with the indicated plasmids for 48 h and then were collected for immunoprecipitation assay with the FLAG tag antibody followed by the immunoblotting analysis with the ubiquitin antibody.

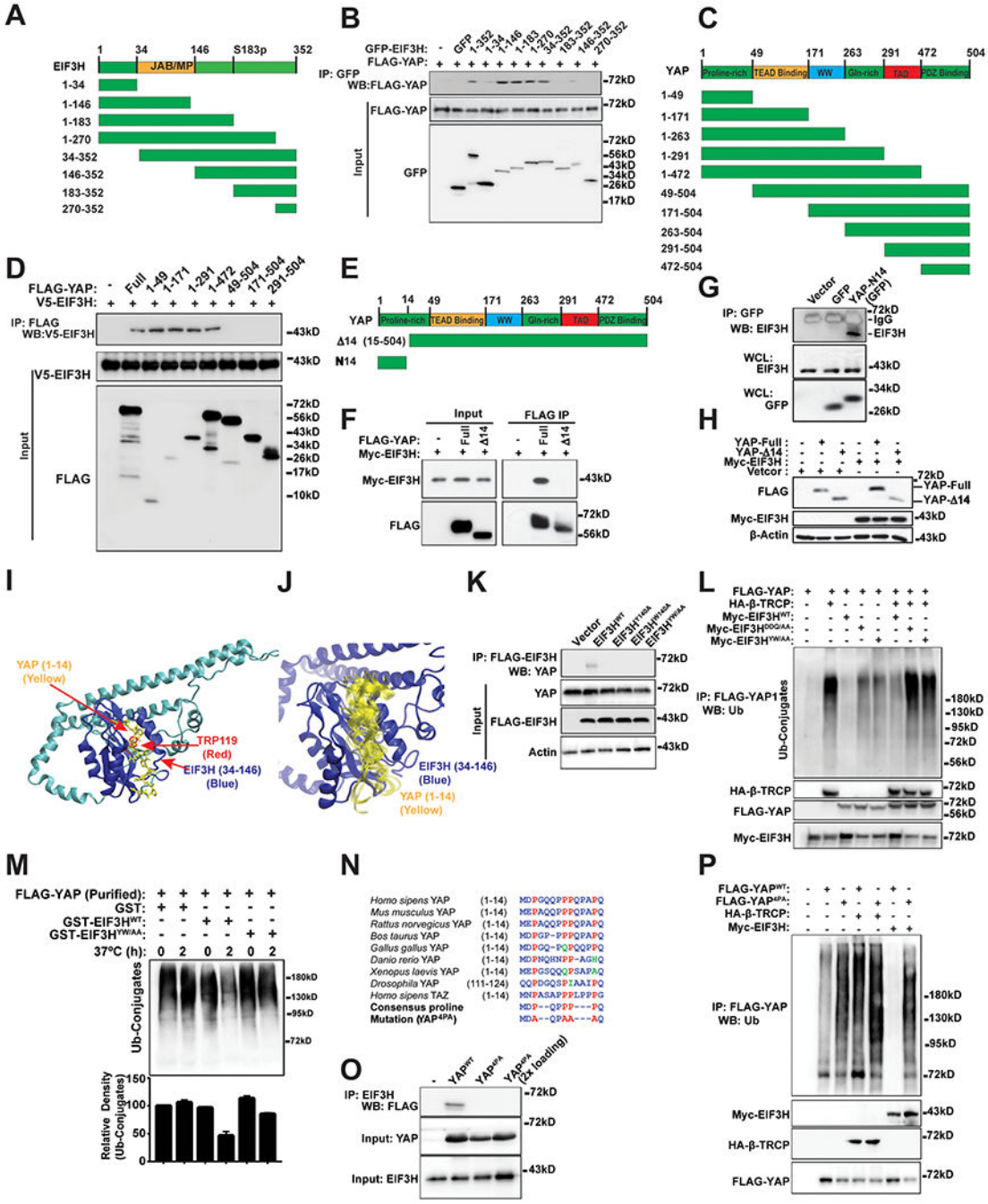

Figure 5. Identification of Tyr140 and Trp119 on EIF3H and Proline-rich motif in YAP N-terminals as critical residues in facilitating the interaction between EIF3H and YAP.

(**A**) Schematic diagram of human EIF3H domains and strategy to engineer a series of EIF3H deletion mutants. (**B**) Identification of amino acid stretch 34–146 on the JAB/MPN domain of EIF3H involved in mediating its interaction with YAP. (**C**) Schematic diagram of human YAP domains. (**D**) Identification amino acid stretch 1–49 on YAP facilitates the interaction between EIF3H and YAP. (**E**) Schematic diagram of human YAP domains and strategy to engineer YAP-N14 and Δ14 (15–504) mutants. (**F**) Loss of the N-terminal amino acid

stretches from 1–14 on YAP failed to co-immunoprecipitated with EIF3H. (**G**) GFP or GFP-N14 (YAP-N14) were transfected into 293 cells and then pulled down with antibody against GFP following by western blotting using the EIF3H antibody. The EIF3H could co-IP with GFP-N14. (**H**) Co-transfection of myc-EIF3H with YAP-full or YAP-Δ14. EIF3H only stabilizes the full-length YAP. (**I**) Molecular docking analysis of the N-terminal 14 amino acids on YAP and the EIF3H catalytic core (34–146 amino acids) which are modelled with the homology modelling service iTASSER. The catalytic core of EIF3H and stretch [1–14] of YAP are shown in *blue* and *yellow*, respectively. (**J**) Ensemble of poses obtained from flexible docking performed with Haddock. (**K**) Measurement of interaction between the wild-type EIF3H or EIF3H^{Y140A}, EIF3H^{W119A}, or EIF3H$^{Y140A/W119A}$ (EIF3H$^{YW/AA}$) with YAP using a coimmunoprecipitation assay. Only the interaction between wild-type EIF3H and YAP was detected. (**L**) FLAG-YAP was co-transfected with Myc tagged wild-type (EIF3H^{WT}) or mutant EIF3H (EIF3H$^{DDQ/AAA}$ and EIF3H$^{YW/AA}$), and then treated with 10 mM MG132 for 4h following by pull-down with FLAG tag antibody. Only the wild-type EIF3H deubiquitinates YAP poly-ubiquitin conjugates catalyzed by β-TRCP/SCF. (**M**) Deubiquitylation of YAP by wild-type and mutant EIF3H (EIF3H$^{YW/AA}$) *in-vitro* using purified FLAG-tagged YAP proteins from transfected HEK293T cells. Only the wild-type EIF3H significantly deubiquitinates YAP poly-ubiquitin conjugates. The down panel is a density analysis of the upper panel. (**N**) Alignment of stretch [1–14] of human YAP crossing multiple species. A mutant YAP (YAP^{4PA}) was engineered with four conserved proline residues replaced by alanine. (**O**) Measurement of interaction between the YAP^{WT} and YAP^{4PA} with EIF3H using a coimmunoprecipitation assay. (**P**) Deubiquitylation of wild-type and mutant YAP by EIF3H. FLAG-YAP or mutant YAP were co-transfected with Myc tagged wild-type EIF3H, and then treated with 10 mM MG132 for 6h following by pull-down with FLAG tag antibody. EIF3H can remove β-TRCP/SCF-mediated poly-ubiquitin conjugates from wild-type YAP, but not YAP^{4PA}.

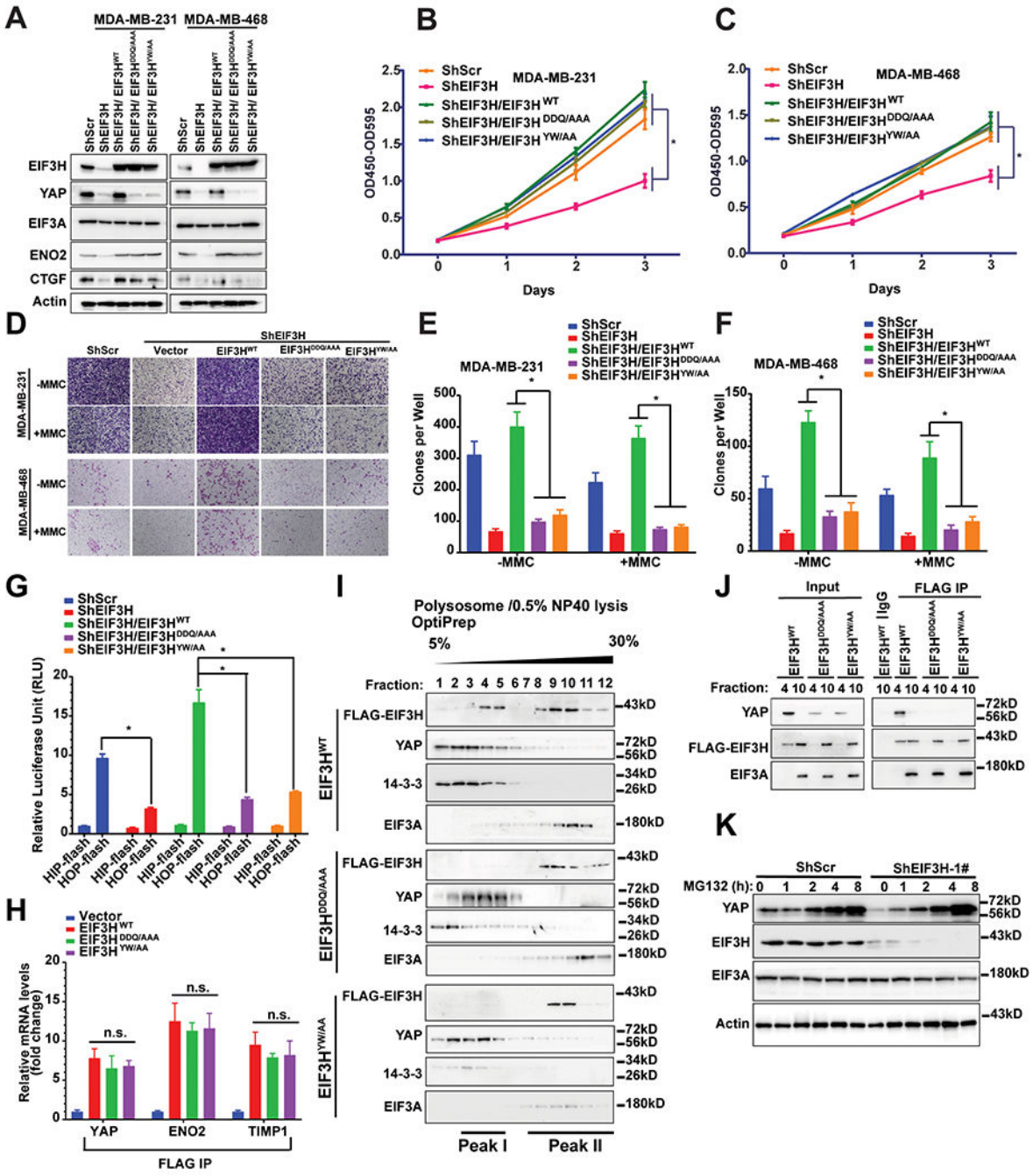

Figure 6. Mutated EIF3H catalytic core or disrupted EIF3H-YAP binding affect YAP expression is independent of translation.

(**A**) Expression of EIF3H, YAP and EIF3A in MDA-MB-231 and MDA-MB-468 cells with EIF3H knockdown and EIF3H^{WT}, EIF3H$^{DDQ/AAA}$ or EIF3H$^{YW/AA}$ add-back. (**B-C**) Cell proliferation assay of MDA-MB-231 (**B**) and MDA-MB-468 (**C**) cells with EIF3H knockdown and EIF3H addback. Error bars represent standard deviation. Mutant EIF3H fully recovery cell proliferation as wildtype EIF3H. (**D-F**) Transwell invasion assay of MDA-MB-231 and MDA-MB-468 cells with EIF3H knockdown and EIF3H addback.

Mutant EIF3H failed recovery cell invasion as wildtype EIF3H. (**D**) Represented image of transwell invasion. (**E**) Summary of MDA-MB-231. (**F**) Summary of MDA-MB-468. MMC, mitomycin C. Error bars represent standard deviation. (**G**) Reporter assay. MDA-MB-231 were transfected with HIP (negative control)-flash and HOP (Hippo-YAP signaling optimal promoter)-flash reporters. Data were obtained from three independent experiments. Error bars represent standard deviation. (**H**) RT-qPCR analysis of EIF3H complex-associated YAP, ENO2 and TIMP1 mRNAs using FLAG tag immunoprecipitation. Data are mean ± s.d. from two independent experiments. n.s., not significant. (**I**) OptiPrep density gradient assay (5%-30%) in MDA-MB-231-EIF3H^{WT}, MDA-MB-231-EIF3H$^{DDQ/AAA}$ and MDA-MB-231-EIF3H$^{YW/AA}$ cells lysates. The wildtype EIF3H has an additional accumulation peak (peak I) in comparison to mutant EIF3H. The 14-3-3 and YAP were accumulated in peak I and EIF3A were accumulated in peak II. (**J**) FLAG tag immunoprecipitation of EIF3H in fraction 4 (peak I) and 10 (peak II). While no difference of EIF3A associated with wildtype or mutant EIF3H in peak 10 (peak II), no YAP protein associated with the mutant EIF3H in fraction 4 (peak I). (**K**) MDA-MB-231-ShEIF3H-1# and control cells were treated with 20μM MG132 for the indicated time. Expression of YAP, EIF3H, EIF3A and Actin was detected by western blot. The asterisks indicated statistical significance ($p<0.05$).

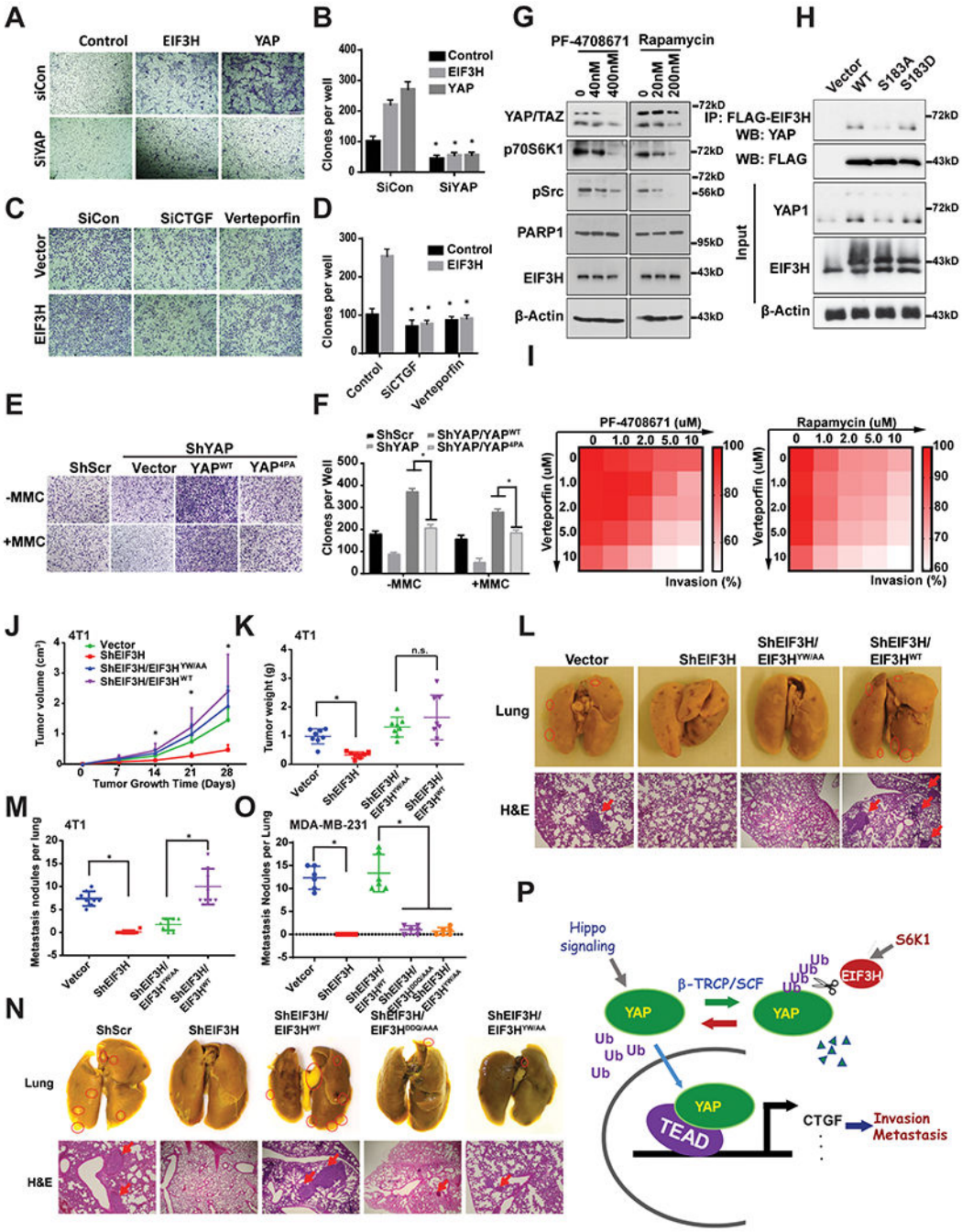

Figure 7. Stabilization of YAP by EIF3H promotes breast cancer invasion and metastasis.

(**A & B**) Depletion of YAP by RNA interference abolishes EIF3H-YAP driven transwell invasion. MDA-MB-231 cells with elevated expression of EIF3H and YAP were transfected with YAP siRNA for 48h and then evaluated for their transwell capability. (**B**) is the statistical result of **A**. (**C & D**) Depletion of CTGF expression or blockade of YAP activity by verteporfin inhibits the transwell invasion driven by EIF3H -YAP in the breast cancer cells. MDA-MB-231-EIF3H cells were transfected with CTGF siRNA for 48h, or treated with 10 μM verteporfin for 24h, following by transwell capability analysis. (**D**) is the

statistical result of **C**. (**E & F**) Replacement of four proline residues on N-terminal YAP attenuates YAP-driven breast tumor cell invasion in MDA-MB-231 cells. (**F**) is the statistical result of **E**. Error bars represent standard deviation. (**G**) Blockade of S6K1 and mTOR cascade promotes YAP degradation. 4T1 cells were treated with PF4708671 and rapamycin with indicated concentrations for 24h and then lysed and subjected to western blotting for measuring EIF3H, YAP, and β-Actin. (**H**) Replacement of Ser183 by Ala on EIF3H leads to reduced interaction between EIF3H and YAP, which further results in the destabilization of YAP. (**I**) Synergized effect of PF4708671 and rapamycin with Verteporfin in the inhibition of the transwell invasion. (**J-M**) 5×10^5 4T1 cells with s.c. injected into the mammary fat pad of Balb/c mice (n=8 per group). (**J**) Tumor growth curve (**J**). (**K**) Tumor weight. While knockdown EIF3H significantly retards 4T1 tumor growth, add back of $EIF3H^{WT}$ or $EIF3H^{YW/AA}$ to 4T1/ShEIF3H has no significant difference in tumor growth. n.s.; not significant. (**L**) The mouse lung and H&E staining of lung section. The upper panel shows the mouse lung image and the metastasis nodules at the surface were indicated by red circles. The down panel shows the H&E staining of lung section and the micrometastasis foci was indicated by red arrows. (**M**) The statistical result of surface metastasis nodules in the lung of 4T1 xenograft tumor. (**N-O**) 5×10^6 MDA-MB-231 were injected into 6 weeks nu/nu mice. 4 months later, the mice were sacrificed and the lungs were sectioned for staining with H/E. (**N**) The upper panel shows the mouse lung image and the metastasis nodules at the surface were indicated by red circles. The down panel shows the H&E staining of the lung section and the micrometastasis foci was indicated by red arrows. (**O**) The statistical result of surface metastasis nodules in the lung. (**P**) Proposed working model for regulation of YAP by EIF3H in orchestrating tumor metastasis. The asterisks indicated statistical significance ($p<0.05$).